Miner Petrol (2011) 102:99–115
DOI 10.1007/s00710-011-0176-4

SPECIAL ISSUE ACCESSORY MINERALS

Pre-Variscan evolution of the Western Tatra Mountains: new insights from U-Pb zircon dating

Jolanta Burda · Urs Klötzli

Received: 30 November 2010 / Accepted: 2 September 2011 / Published online: 27 September 2011

Abstract In situ LA-MC-ICP-MS U-Pb zircon geochronology combined with cathodoluminescence imaging were carried out to determine protolith and metamorphic ages of orthogneisses from the Western Tatra Mountains (Central Western Carpathians). The metamorphic complex is subdivided into two units (the Lower Unit and the Upper Unit). Orthogneisses of the Lower Unit are mostly banded, fine- to medium-grained rocks while in the Upper Unit varieties with augen structures predominate. Orthogneisses show a dynamically recrystallised mineral assemblage of Qz+Pl+Bt±Grt with accessory zircon and apatite. They are peraluminous (ASI=1.20–1.27) and interpreted to belong to a high-K calc-alkaline suite of a VAG–type tectonic setting. LA-MC-ICP-MS U-Pb zircon data from samples from both units, from crystals with oscillatory zoning and Th/U>0.1, yield similar concordia ages of ca. 534 Ma. This is interpreted to reflect the magmatic crystallization age of igneous precursors. These oldest meta-magmatics so far dated in the Western Tatra Mountains could be linked to the fragmentation of the northern margin of Gondwana. In zircons from a gneiss from the Upper Unit, cores with well-developed oscillatory zoning are surrounded by weakly luminescent, low contrast rims (Th/U<0.1). These yield a concordia age of ca. 387 Ma corresponding to a subsequent, Eo-Variscan, high-grade metamorphic event, connected with the formation of crustal-scale nappe structures and collision-related magmatism.

Editorial handling: F. Finger and D. Harlov

J. Burda (✉)
Faculty of Earth Sciences, University of Silesia,
Sosnowiec, Poland
e-mail: jolanta.burda@us.edu.pl

U. Klötzli
Department of Lithospheric Research, University of Vienna,
Vienna, Austria

Introduction

The Proterozoic to late Palaeozoic evolution of the Central Western Carpathians (CWC) has an important bearing on the reconstruction of the geological development of Central Europe. However, due to shortcomings in the knowledge of the temporal evolution of the series involved, the area of the CWC is often not considered in tectonic and palaeogeographic reconstructions of the pre-Alpine development of the region.

The crystalline basement of the Tatra Mountains is one of several Variscan crystalline complexes of the CWC, only weakly affected by Alpine overprint (Krist et al. 1992). This is very favourable for the reconstruction of the sequence of pre-Alpine events, however, our knowledge of the pre-Mesozoic evolution of the Tatra Mountains is still far from complete. Therefore, for a more detailed reconstruction of the evolution of basement rocks of the Tatra Mountains and for the comparison with the tectonic history of other crystalline basement units of the CWC, more studies of metamorphic rocks are needed.

Among accessory phases, zircon has proven particularly suitable for tracking the evolution of metamorphic terrains with complex polyphase development, because its internal structures are directly correlated with chemical, isotopic and geochronologicall information encoded within individual grains (e.g. Griffin et al. 2002; Rubatto 2002; Whitehouse and Platt 2003; Hoskin 2005). The U-Pb dating of zircons is presently one of the most powerful tools for revealing the evolution of geological units. Determination of the zircon age spectrum from polygenetic metamorphic and magmatic complexes is a complicated task, because zircon crystals often record a succession of different geological events. The main advantages of U-Pb zircon geochronology using the laser ablation ICP-MS is a relatively small spot size

(<30 μm), which allows the collection of data from different growth zones revealed previously by detailed cathodoluminescence (CL) investigations.

Because there is no general consensus about the pre-Variscan geodynamic evolution of the metamorphic basement of the Tatra Mountains we have tried to determine the protolith ages of gneisses representing both structural units of the crystalline basement. Detailed investigation of zircon morphology, internal structures and chemical variations helped to interpret the U-Pb zircon data of the analyzed rocks.

Geological setting

The crystalline core of the Tatra Mountains belongs to the basement of the Tatric Unit in the CWC, which is one of the disrupted fragments of the Variscan orogen spread in Central and Eastern Europe. The crystalline basement of the Tatra Mountains comprises metamorphic rocks and Variscan granitoids, overlain by Mesozoic and Cenozoic sedimentary successions (Fig. 1).

The metamorphic envelope of the Variscan granidoids cropping out in the western part of the massif (Fig. 1) is subdivided into two units, the Lower Unit and the Upper Unit, both with different lithologies and metamorphic grades (Kohút and Janak 1994; Gawęda et al. 1998).

The Lower Unit consists of mica schists, gneisses and minor amphibolites. The peak metamorphic conditions were estimated at T=550–600°C and P=5–8 kbar (Kohút and Janak 1994; Gawęda et al. 1998). This unit was considered to represent a continuous volcano-sedimentary succession of early Palaeozoic age (Kohút et al. 2008).

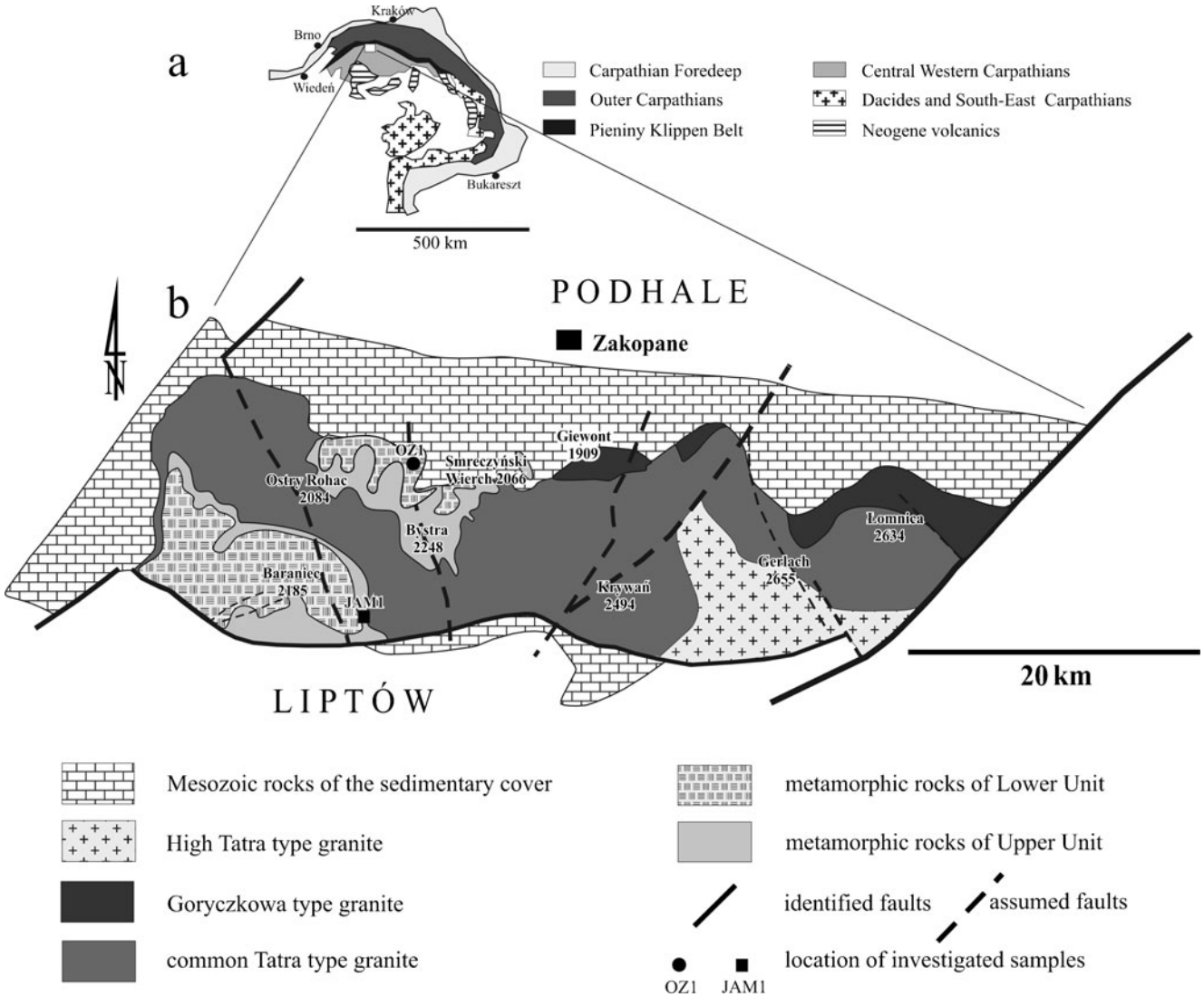

Fig. 1 The geology of the Tatra Mountains. **a** Simplified geological sketch of the Carpathian chain. **b** Geological map of the Tatra Mountains Block (after Kohút and Janak 1994; Bac-Moszaszwili 1996; Gawęda et al. 2005)

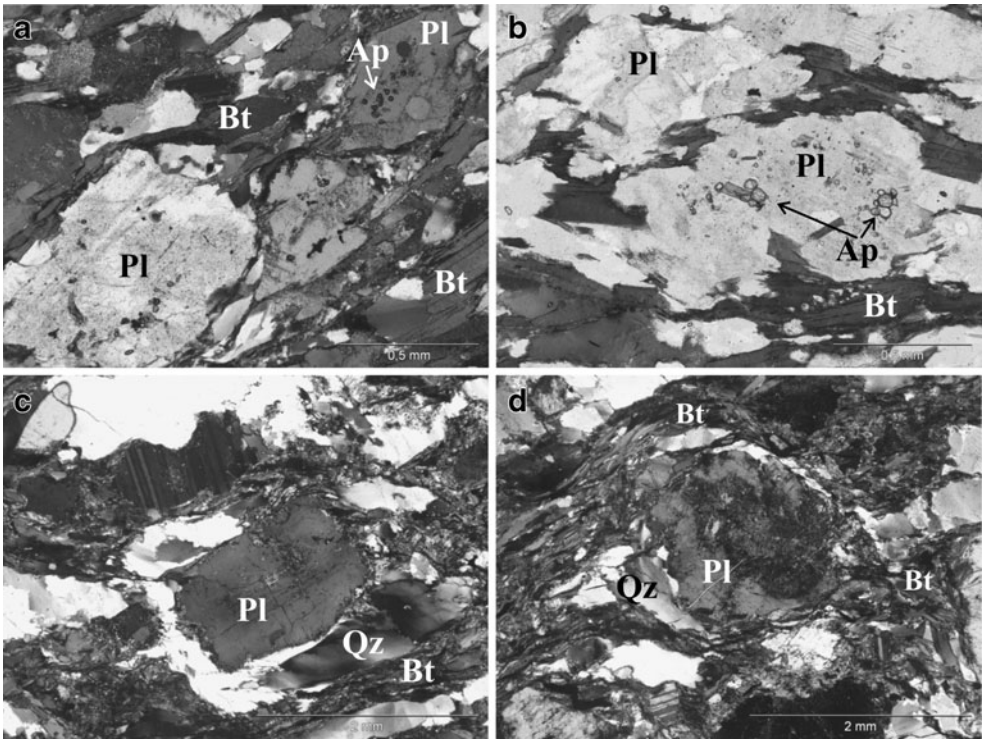

Fig. 2 Microphotographs of orthogneisses from the Western Tatra Mountains: **a**, **b** typical microfabrics of orthogneisses from the Lower Unit (sample OZ1); **b**, **c** augen-banded structures of orthogneisses from the Upper Unit (sample (JAM1); plagioclase porphyroclast with tails of deformed and dynamically recrystallized margins; **a**, **c**, **d** crossed nicols; **b** parallel nicols; Abbreviations: *Ap* apatite; *Bt* biotite; *Pl* plagioclase; *Qz* quartz

The Upper Unit is composed of migmatitic rocks: gneisses and amphibolites, graphite quartzites and subordinate intercalations of mica schists (Burda and Gawęda 1997, 1999; Gawęda et al. 2000). The peak of metamorphism in this unit was under upper amphibolite facies conditions (T=690–780°C, P=7.5–10 kbar; Kohút and Janak 1994; Gawęda et al. 1998). Locally, eclogitic remnants, most probably tectonically emplaced, are present among predominantly metapelitic lithologies (Janák et al. 1996). These metamorphic sequences were

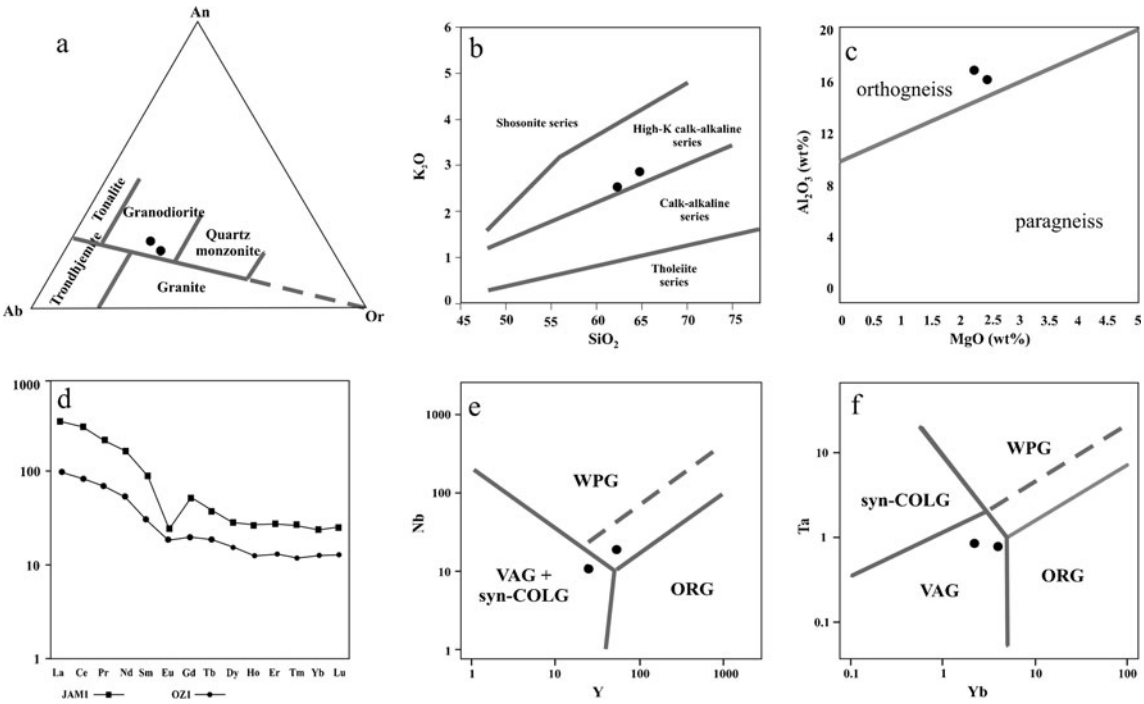

Fig. 3 Major and trace element plots for the Western Tatra orthogneisses. **a** normative anorthite–albite–orthoclase plot (O'Connor 1965); **b** K_2O versus SiO_2 plot; **c** Al_2O_3 versus MgO plot (Marc 1992); **d** rare earth elements patterns normalized to C1 chondrite (Sun and McDonough 1989); **e**, **f** Pearce et al. (1984) discrimination diagrams for the tectonic setting of granitoid rocks

intruded by Variscan polygenic granitoids, emplaced in the following sequence: (1) intrusion of the older Tatra granite, now present as orthogneisses - dated at ca. 405 Ma (Poller et al. 2000); (2) formation of subduction-related granodiorites-tonalites - called the common Tatra type granite, around 350–360 Ma (Poller et al. 2000, 2001a,b); (3) formation of leucogranites of the same age (360 Ma), resulting from partial melting of the metamorphic complex during thrusting and metamorphic inversion (Burda and Gawęda 2009); (4) intrusions of quartz diorites (ca. 341 Ma) found as small dykes and sills cutting the metamorphic rocks (Poller et al. 2000; Gawęda et al. 2005), and (5) dominantly in the eastern part - porphyritic granodiorite and equigranular biotite monzo- to syenogranites (called the High Tatra type) intruded at ca. 314 Ma (Poller et al. 2000). In the northern part of the massif, the so called Goryczkowa type granites (356±8 Ma) occur only as "crystalline islands", forming the cores of the Alpine Mesozoic nappes (e.g. Burchard 1968; Kohút and Janak 1994; Burda and Klötzli 2007).

Analytical techniques

Two samples of gneisses from the Lower and Upper Unit, each of approximate 25 kg were collected for the investigations. Whole- rock analyses of major and trace elements were carried out by XRF and ICP-MS methods in the ACME Analytical Laboratories, Vancouver, Canada. Zircon crystals were separated using standard techniques involving crushing, hydrofracturing, washing, Wilfley table, magnetic separator and handpicking. Approximately 50 zircon grains from each sample were selected for morphological studies by scanning electron microscopy (SEM). Then they were mounted in epoxy and polished to expose the centers of the grains. Zircon crystals were imaged by cathodoluminescence (CL) using a FET Philips XL 30 electron microscope (15 kV and 1 nA) at the University of Silesia, Sosnowiec.

Zircon $^{206}Pb/^{238}U$ and $^{207}Pb/^{206}Pb$ ages were determined using a 193 nm solid state Nd-YAG laser (NewWave UP193-SS) coupled to a multi-collector ICP-MS (Nu Instruments HR) at the University of Vienna. Ablation in a He atmosphere was either spot- or raster-wise according to the CL zonation pattern of the zircons. Spot analyses were 15–25 μm in diameter whereas line widths for rastering were 10–15 μm with a rastering speed of 5 μm/s. Energy densities were 5–8 J/cm^2 with a repetition rate of 10 Hz. The He carrier gas was mixed with the Ar carrier gas flow prior to the plasma torch. Ablation duration was 60 to 120 s with a 30 s gas and Hg blank count rate measurement preceding ablation. Ablation

Table 1 Chemical composition of the representative samples of orthogneisses from the Western Tatra Mountains. Major elements in mass%, trace elements in ppm; A/CNK – molar $Al_2O_3/(CaO+Na_2O+K_2O)$; LOI - loss on ignition; $Eu/Eu^* = Eu/\sqrt{Sm \times Gd}$

Sample	OZ1	JAM1
SiO_2	64.84	62.49
TiO_2	0.72	0.85
Al_2O_3	15.87	16.62
Fe_2O_3	6.14	6.81
MnO	0.09	0.11
MgO	2.46	2.29
CaO	2.37	2.79
Na_2O	3.49	3.58
K_2O	2.86	2.38
P_2O_5	0.13	0.05
LOI	0.9	1.7
Total	99.87	99.67
A/CNK	1.21	1.22
La	25.7	90.9
Ce	57.5	204.6
Pr	7.04	22.98
Nd	11.2	86.5
Sm	5.1	15.21
Eu	1.21	1.5
Gd	4.59	11.75
Tb	0.74	1.52
Dy	4.21	7.8
Ho	0.76	1.62
Er	2.35	4.9
Tm	0.33	0.74
Yb	2.22	4.51
Lu	0.34	0.71
Total REE	123	455
Eu/Eu*	0.76	0.34
La_N/Yb_N	8.3	14.4
Gd_N/Yb_N	1.7	12.5
Sr	337	311
Ba	567	657
Rb	96	92
Be	1	1
Th	8.4	37.5
U	1.8	1.8
Ni	38.1	18.4
Ga	20.1	21.6
V	109	106
Zr	184	315
Hf	5.5	8.5
Y	24	45
Nb	11	15
Ta	0.7	0.7
Zr/Hf	34	37
Nd/Th	0.30	2.31
Rb/Sr	0.28	0.30

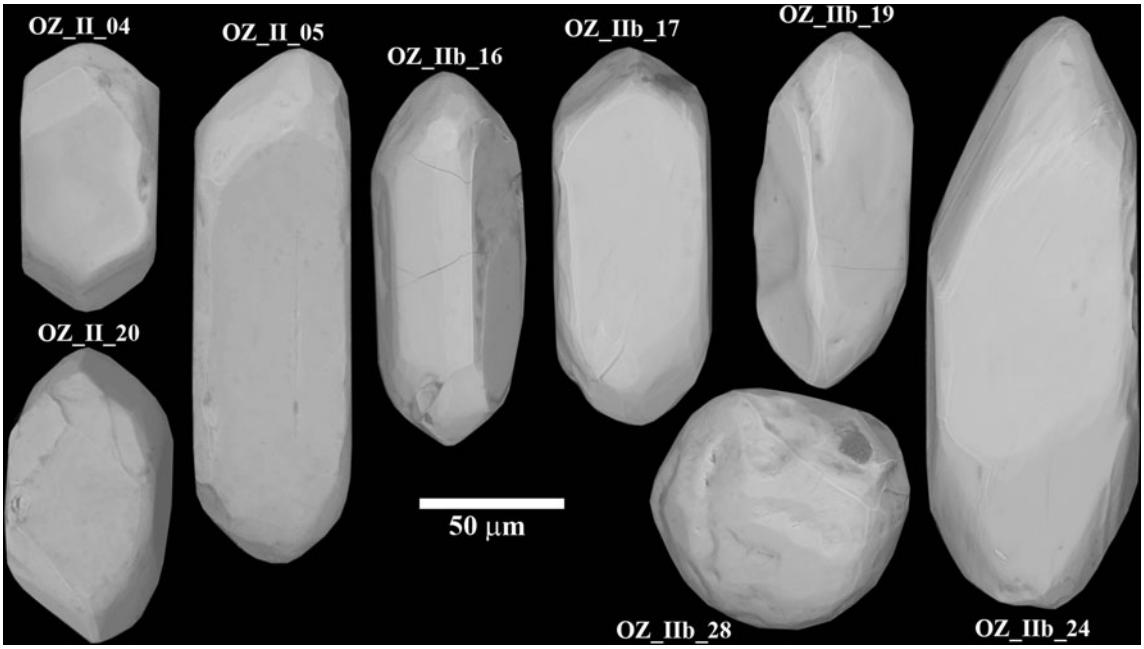

Fig. 4 Secondary electron (SEM) images of zircon crystals from orthogneiss OZ1 from the Lower Unit. Most crystals show a predominance of [110] prism and the presence of two pyramids [101, 211]

count rates were corrected accordingly offline. Remaining counts on mass 204 were interpreted as representing ^{204}Pb. Static mass spectrometer analysis was as follows: ^{238}U in a Faraday detector, ^{207}Pb, ^{206}Pb, and 204 (Pb+Hg) were in ion counter detectors. ^{208}Pb was not analysed. An integration time of 1 s was used for all measurements. The ion counter – Faraday and inter-ion counter gain factors were determined before the analytical session using standard zircons 91500 (Wiedenbeck et al. 1995) and Plesovice (Slama et al. 2006). Sensitivity for ^{206}Pb on standard zircon 91500 was c. 30'000cps per ppm Pb. For ^{238}U the corresponding value was c. 35'000.

Mass and elemental bias and mass spectrometer drift of both U/Pb and Pb/Pb ratios, respectively, were corrected using a multi-step approach: first-order mass bias is corrected using a desolvated ^{233}U-^{205}Tl-^{203}Tl spike solution which is aspirated continuously in Ar and mixed to the He carrier gas coming from the laser before entering the plasma. This corrects for bias effects stemming from the mass spectrometer. The strongly time-dependent elemental fractionation coming from the ablation process itself is then corrected for using the "intercept method" of Sylvester and Ghaderi (1997). The calculated ^{206}Pb/^{238}U and ^{207}Pb/^{206}Pb intercept values are corrected for mass discrimination from analyses of standards 91500 and Plesovice measured during the analytical session using a standard bracketing method. The correction utilizes regression of standard measurements by a quadratic function. A common Pb correction was applied to the final data using the apparent ^{207}Pb/^{206}Pb age and the Stacey and Kramers (1975) Pb evolution model. The final U/Pb ages were calculated at 2σ standard deviation using the Isoplot/Ex program - version 3.00 (Ludwig 2003).

The microprobe analyses of separated zircons were carried out on CAMECA SX-100 microprobe analyzer equipped with 3 wavelength-dispersive spectrometers in the Inter-Institution Laboratory of Microanalyses of Minerals and Synthetic Substances at the University of Warsaw. The operating conditions were: acceleration voltage −20 kV, beam current −50 nA and beam diameter −2 μm.

Mineral abbreviations used here follow these proposed by Whitney and Evans (2010).

Sample description

The sample from the Lower Unit (OZ1) was collected at Ornaczański Żleb and the sample from the Upper Unit (JAM1) from Jamnicka Valley (Fig. 1b).

Sample OZ1 is a dark and strongly foliated, fine-grained granodioritic orthogneiss. It is composed mainly of plagioclase (An_{26-31}), biotite, minor K-feldspar and quartz. Accessory minerals include zircon, titanite, rutile, apatite and ilmenite. The rock shows a strong penetrative foliation, defined mainly by biotite. (Fig. 2a, b).

Sample JAM1 is a strongly foliated, grey granodioritic augen-gneiss with an S-C fabric (Fig. 2c, d). It is composed of aligned dynamically recrystallised quartz, plagioclase

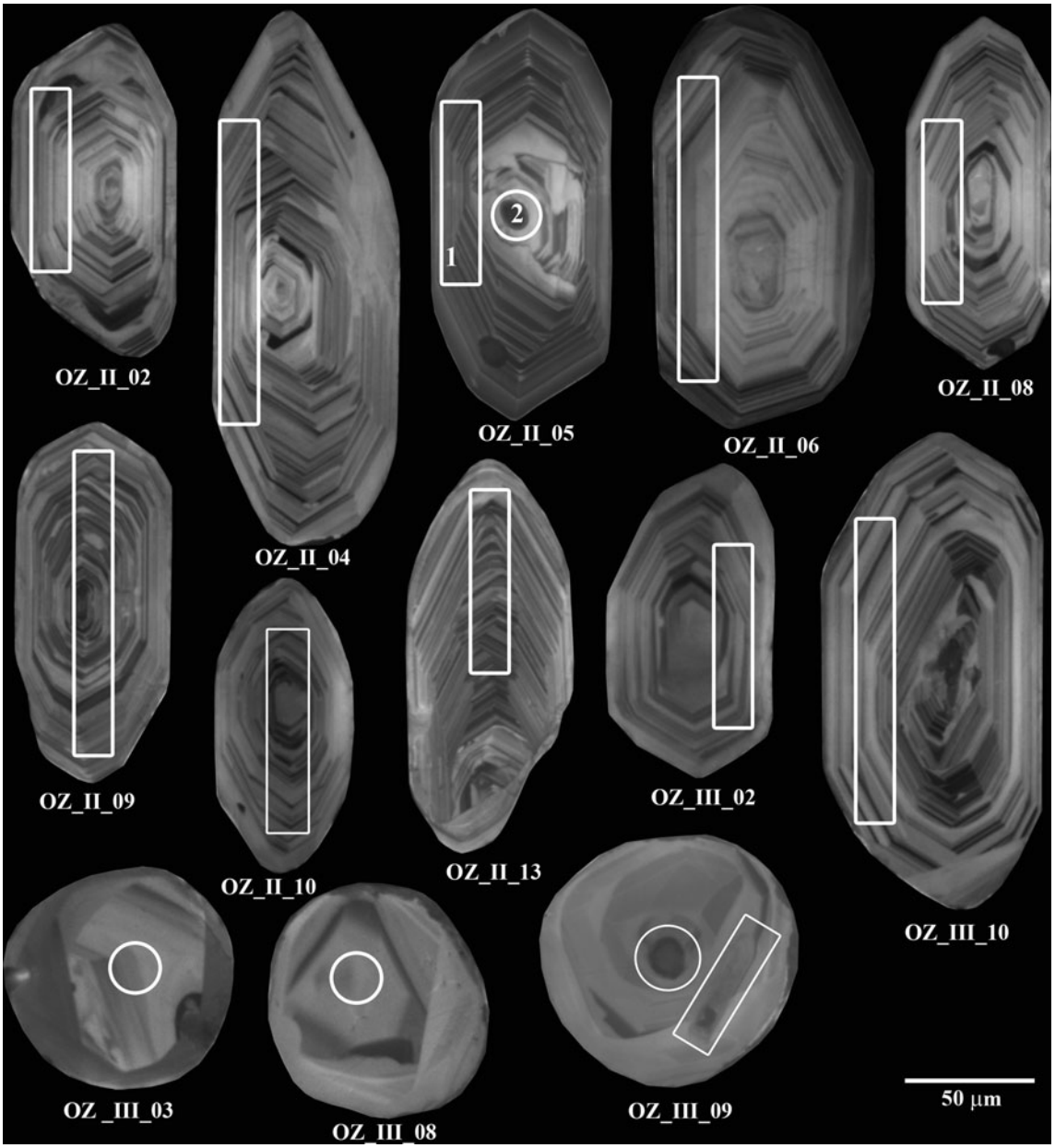

Fig. 5 Cathodoluminescence images of characteristic zircon populations from orthogneiss OZ1. See text for description. The white rectangles and circles show the approximate location of laser ablation trenches and are not to scale

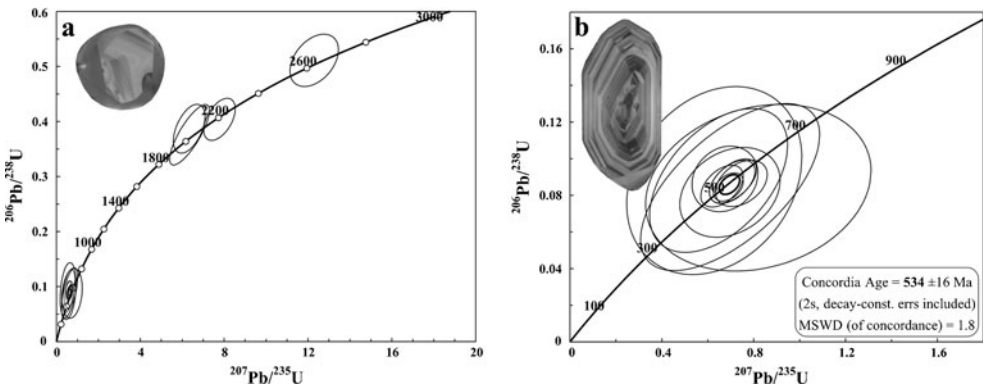

Fig. 6 Concordia plots of LA-MC-ICP-MS U-Pb zircon analytical results from orthogneiss OZ1. Open error ellipses are isotope ratios of individual grain spots on xenocrysts (**a**) and oscillatory zoned zircons (**b**). Thick error ellipse correspond to the 2σ and 95% confidence errors of the calculated concordia ages

Table 2 U-Pb analytical results from zircons of orthogneiss OZ1 from the Lower Unit

File name	Final blank corrected intensities				Final mass bias and common Pb corrected ratios						
	$^{204}Pb^{a}$	$^{206}Pb^{b}$	$^{207}Pb^{b}$	$^{238}U^{b}$	$^{207}Pb/^{206}Pb$	2RSE (%)	$^{207}Pb/^{235}U$	2RSE (%)	$^{206}Pb/^{238}U$	2RSE (%)	Rho
OZ1_II_02	1.28	0.32	0.03	8.86	0.0603	7.5	0.6959	7.5	0.0833	7.5	0.40
OZ1_II_04	0.81	0.21	0.02	5.75	0.0527	48.8	0.6339	48.8	0.0871	48.8	0.25
OZ1_II_05/1	1.04	0.15	0.01	4.46	0.0624	25.3	0.7022	25.3	0.0804	25.2	0.27
OZ1_II_05/2	0.88	0.60	0.05	16.48	0.0565	11.2	0.6678	11.2	0.0840	11.2	0.47
OZ1_II_06	0.81	0.23	0.02	6.30	0.0627	12.2	0.7507	12.2	0.0855	12.2	0.37
OZ1_II_08	1.71	0.28	0.03	8.03	0.0692	45.8	0.8239	48.4	0.0830	45.3	0.20
OZ1_II_09	0.65	0.35	0.03	9.67	0.0585	11.2	0.7122	11.3	0.0864	11.3	0.50
OZ1_II_10	0.50	0.48	0.04	13.10	0.0580	11.5	0.7149	11.5	0.0868	11.5	0.53
OZ1_II_13	0.52	0.22	0.02	5.90	0.0577	44.8	0.7017	45.1	0.0833	45.2	0.63
OZ1_III_02	0.82	0.26	0.02	5.07	0.0566	17.0	0.6799	17.1	0.0878	17.0	0.17
OZ1_III_03	0.97	9.29	2.04	33.84	0.1700	7.6	12.2814	7.7	0.5111	7.6	0.40
OZ1_III_08	1.25	0.76	0.12	3.90	0.1340	7.6	7.8042	7.8	0.4022	7.8	0.50
OZ1_III_09/1	1.72	4.29	0.66	20.16	0.1243	12.0	6.3729	12.0	0.3743	12.1	0.80
OZ1_III_09/2	0.84	2.52	0.39	13.23	0.1214	9.5	6.3550	9.6	0.3854	9.6	0.50
OZ1_III_10	0.89	0.25	0.02	4.97	0.0578	37.0	0.6514	37.4	0.0872	37.2	0.48

Explanations: [a] final blank corrected intensities in μV; [b] final blank corrected intensities in mV; *2RSE* 2-sigma relative standard error (in %); *Rho* the error-correlation between the 206/238 and 207/235 ratios

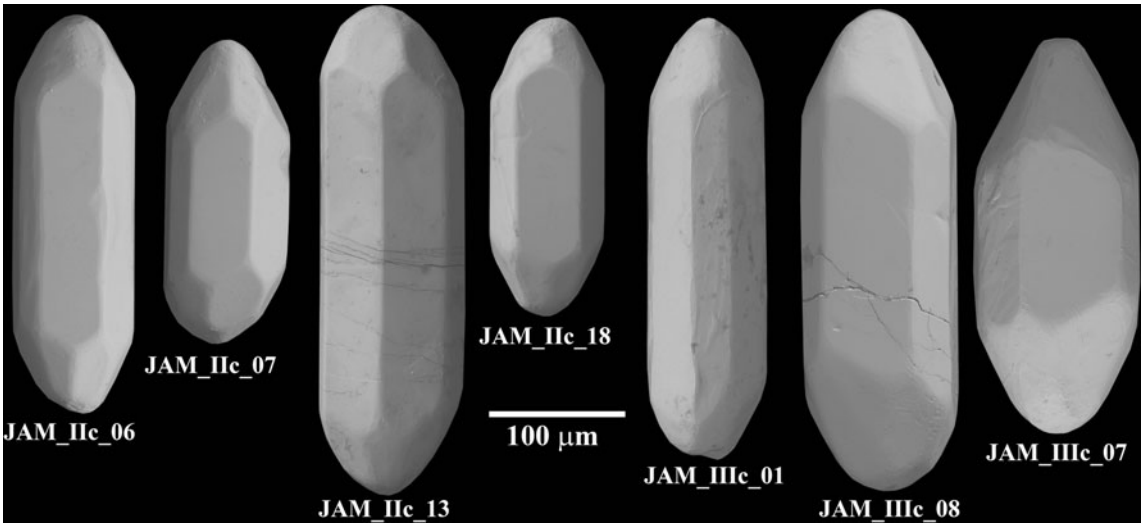

Fig. 7 Secondary electron (SEM) images of zircon crystals from orthogneiss JAM1 from the Upper Unit. Zircon crystals are characterized by dominant [100] and [101] prisms and [211] pyramid

and biotite, with zircon, apatite, Ce-monazite, garnet and ilmenite as accessories.

For both samples, the normative anorthite–albite–orthoclase diagram (O'Connor 1965) indicates granodioritic compositions (Fig. 3a) and both plot in the high-K calc-alkaline field of the K_2O versus SiO_2 diagram (Fig. 3b). The peraluminous character of the orthogneisses is indicated by the molar proportion A/CNK=1.2 (Table 1) and by the CIPW normative corundum value of 3.0–3.2. An Al_2O_3 versus MgO diagram (Marc 1992) shows that the samples fall in the orthogneiss field (Fig. 3c). The REE patterns revealed some differences between the two samples (Fig. 3d). The REE patterns of sample JAM1 is moderately enriched in the LREE (La_N/Yb_N=13), and shows a more pronounced negative Eu anomaly (Eu*= 0.34). In contrast, sample OZ1 shows a less enriched REE pattern (La_N/Yb_N=7.8) with a smaller negative Eu anomaly (Eu*=0.76). In the Nb-Y trace–element discrimination diagram of Pearce et al. (1984), sample JAM1 plots in the field of within-plate granitoids (WPG), while the sample OZ1 plots in the syn-COLG/VAG field (Fig. 3e). Using the Ta vs. Yb discrimination diagram (Pearce et al. 1984), both samples plot in the field of volcanic arc granitoids (VAG, Fig. 3f).

Zircon characteristics and U-Pb dating

Sample OZ1

Zircon crystals are generally subhedral, clear and colourless. The grain size varies from ca. 50 to 300 μm in length (Fig. 4). The crystal termination may appear rounded, but some grains have visible, multiple faces. There are two main morphological types of zircons present in the sample (Fig. 4). Most zircon grains (54%) are normal prismatic (mean elongation ca. 2.5). CL investigations of these crystals show only magmatic oscillatory zoning (Fig. 5, 1st- 2nd row) with a Th/U ratio ranging from 0.2 to 0.7. These crystals have a clearly magmatic origin, with no evidence of metamorphic reworking, suggesting that all zircons of this morphological type grew at the same conditions. Less abundant, isometric crystals exhibit two different domains: an internal part with sector zoning (Th/U ratio from 0.13 to 0.2) surrounded by a rim, showing weak luminescence and Th/U<0.1 (Fig. 5, 3 rd row).

U-Pb isotopic data obtained by the LA-MC-ICP-MS analysis of ten zircons with centre to margin oscillatory growth zones yield a concordia age of 535±16 Ma (MSWD= 1.8) (Fig. 6b, Table 2), which is interpreted to reflect the time of crystallization of the gneiss protolith. Three isometric crystals yielded significantly older, concordant ages at ca. 2.0, 2.2, and 2.6 Ga (Fig. 6a, Table 2). These are interpreted as xenocrysts, probably inherited from the source-rock of the magma.

Sample JAM1

Zircons are mainly colourless, euhedral to subhedral, normal to long prismatic, with aspect ratios of 1:3 to 1:5. The characteristic feature of these zircons is high content (38%) of long prismatic (length-to-width ratio>4) crystals. Grain size varies in length from ca. 100 to 350 μm (Fig. 7). For most grains, CL images (Fig. 8) reveal an euhedral zoned innermost part (core) with Th/U>0.1, surrounded by a weakly luminescent, low contrast rim (Th/U<0.1). The cores display a narrowly spaced regular oscillatory zoning, which is ascribed to the zircon growth in the protolithic

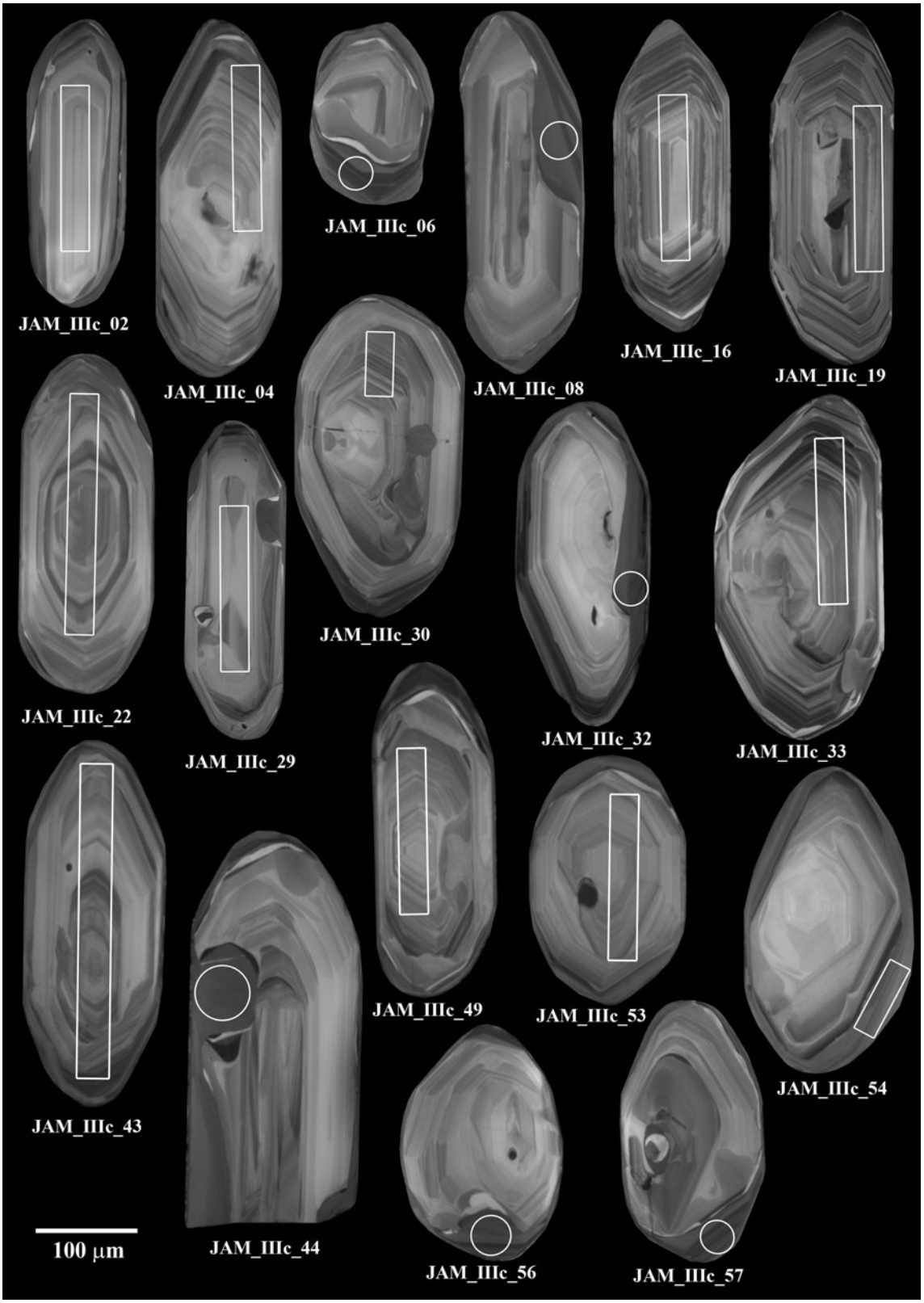

Fig. 8 Cathodoluminescence images of characteristic zircon populations from orthogneiss JAM1. See text for description. The white rectangles and circles show the approximate location of laser ablation trenches and are not to scale

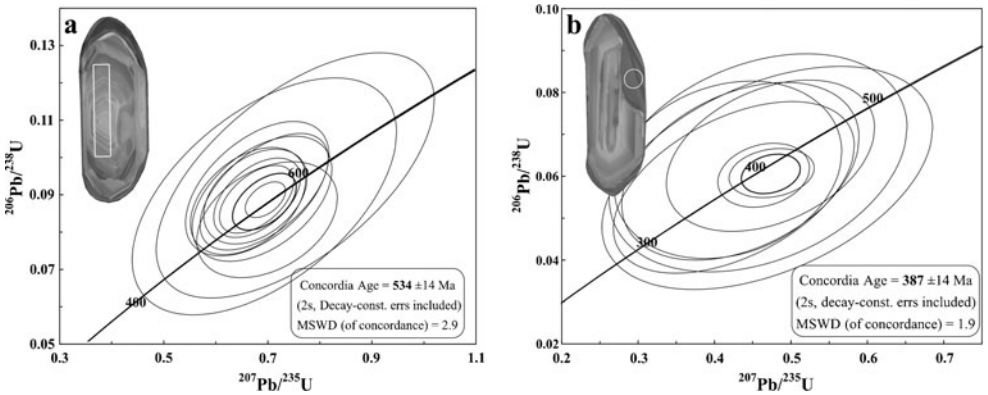

Fig. 9 Concordia plots of LA-MC-ICP-MS U-Pb zircon analytical results from orthogneiss JAM1. Open error ellipses indicate individual spot analysis from igneous zones (**a**) and metamorphic overgrowths (**b**). Thick error ellipse correspond to the 2σ and 95% confidence errors of the calculated concordia ages

melt. In some grains, an irregular, strongly luminescent boundary between these two domains is present (e.g. zircon 06, 44, 49 on Fig. 8). Smoothly rounded dissolution surfaces mark a change in conditions of crystallization involving zircon dissolution followed by later recrystallization of weakly oscillatory zoned outer rims (Fig. 8).

Isotopic data for 18 zircon analyses of 16 grains include 11 analyses of oscillatory zoned interior domains (cores) and seven analyses of exterior domains (rims). Because of small width, the bright seams present between core and rim could not be analysed. The interior domains define a concordia age of 534±16 Ma (MSWD=2.9), interpreted as the magmatic crystallization age of igneous precursor (Table 3, Fig. 9a). The exterior zircon domains give a concordia age of 387±14 Ma (MSWD=1.9) and could represent a subsequent high-grade metamorphic event, constrained by partial recrystallization of primary magmatic zircon and growth of new zircon rims (Table 3, Fig. 9b).

Zircon microprobe analysis

All analyses were performed on sections parallel to the c axis (Fig. 10). A common feature of all zircons from both samples is similar compositional ranges of SiO_2, ZrO_2, HfO_2, Y_2O_3, ThO_2 and UO_2 (Fig. 11, Tables 4 and 5). Only the P_2O_5 contents reach higher values in sample JAM1 (Fig. 11, Tables 4 and 5). The compositional zoning in the analysed zircon generally shows the same trend, defined by an increase in Hf and decrease in U, Th, Y from early to late growth stages of magmatic zircons (Fig. 10). In the late stages of zircon (JAM1) growth, the contents of U, Th, Y and Hf consequently increased (Fig. 10). A positive correlation between P and Y, suggesting the xenotime-type substitution $Zr^{4+}+Si^{4+}\leftrightarrow(Y, REE)^{3+}+P^{5+}$ is observed in zircon from both samples (Tables 4 and 5). The analyses from magmatic domains in the meta-igneous zircons (OZ1, JAM1 core) have Th/U ratio>0.1. The overgrowths in JAM1 are lacking any regular zonation pattern and have a very low Th/U (< 0.1) ratio as is often observed in zircons from amphibolite to granulite facies rocks (Williams et al. 1996; Vavra et al. 1999; Rubatto 2002).

The Zr/Hf ratio displays a large variation, even at the scale of a single crystal. In some grains of zircon from the sample OZ1, the Zr/Hf ratios show a range of 20–67. In zircons from sample JAM1, the Zr/Hf ranges from 31 to 51 (Tables 4 and 5, see Appendix).

Discussion

The orthogneisses from the Western Tatra Mountains correspond to peraluminous, high-K calc-alkaline granites. The value of normative corundum (>1) as well as the molar proportion of $Al_2O_3/CaO+Na_2O+K_2O>1.1$ are indicative of S-type granites (Chappell and White 1974). The emplacement setting of the granites is problematic, although their geochemical features are typical of a volcanic arc environment. Most of the discrimination diagrams are based on Rb, an element which can be very mobile during metamorphism. Without further data that would allow verification of the interpretation based on the geochemical signature, the emplacement setting of the gneiss protoliths is difficult to identify.

SEM and CL analyses of most of the zircons from the gneiss samples from the Western Tatra Mountains show magmatic zonation and typical igneous characteristics. The well preserved euhedral shape of the zircons excludes sedimentary transport. Although many grains have metamorphic overgrowths, the magmatic interiors are not truncated as in detrital populations. The lack of the fragmented zircon crystals also suggests an igneous protolith.

These orthogneisses have zircon Zr/Hf ratios with the same range as that of zircons from crustal sources (Pérez-Soba et al. 2007), supporting the hypothesis that these rocks were derived mainly from recycled crustal rocks.

We have observed a slight decrease in most trace elements (U, Th and Y) from early to late growth stages of magmatic zircons (Fig. 10). The contrasting

Table 3 U-Pb analytical results from zircons of orthogneiss JAM1 from the Upper Unit. *c* core; *r* rim

File name	Final blank corrected intensities				Final mass bias and common Pb corrected ratios						
	$^{204}Pb^a$	$^{206}Pb^b$	$^{207}Pb^b$	$^{238}U^b$	$^{207}Pb/^{206}Pb$	2RSE (%)	$^{207}Pb/^{235}U$	2RSE (%)	$^{206}Pb/^{238}U$	2RSE (%)	Rho
JAM_IIIc_02/c	1.70	2.84	0.14	33.91	0.0557	7.1	0.6799	8.5	0.0884	8.5	0.52
JAM_IIIc_04/c	1.91	4.06	0.20	48.80	0.0556	11.9	0.6946	14.3	0.0904	14.3	0.57
JAM_IIIc_08/r	2.07	0.63	0.03	11.28	0.0566	41.2	0.4688	37.1	0.0595	37.1	0.44
JAM_IIIc_09/r	0.54	0.47	0.02	8.31	0.0495	31.7	0.4186	28.6	0.0614	28.5	0.20
JAM_IIIc_18/c	1.02	3.38	0.16	42.20	0.0557	13.6	0.6815	16.4	0.0912	16.4	0.51
JAM_IIIc_19/c	1.80	1.36	0.07	14.54	0.0551	8.3	0.6811	9.9	0.0888	9.9	0.50
JAM_IIIc_22/c	1.41	1.86	0.09	23.34	0.0570	13.1	0.6904	15.8	0.0885	15.7	0.47
JAM_IIIc_29/c	1.38	0.65	0.03	8.32	0.0612	13.0	0.7004	15.6	0.0828	15.6	0.37
JAM_IIIc_30/c	2.54	1.77	0.09	22.00	0.0574	6.0	0.6950	7.2	0.0877	7.2	0.51
JAM_IIIc_32/r	1.13	1.57	0.08	27.00	0.0516	31.9	0.4344	28.7	0.0611	28.7	0.38
JAM_IIIc_33/c	0.47	1.05	0.05	13.16	0.0548	11.3	0.6642	13.6	0.0879	13.6	0.42
JAM_IIIc_43/c	0.74	1.90	0.10	23.35	0.0559	24.7	0.6953	29.6	0.0892	29.6	0.54
JAM_IIIc_44/r	0.69	0.38	0.02	6.23	0.0523	37.9	0.4573	34.3	0.0631	34.1	0.33
JAM_IIIc_49/c	1.35	1.41	0.07	17.15	0.0556	9.9	0.6783	11.9	0.0891	11.9	0.39
JAM_IIIc_53/c	1.06	1.46	0.07	17.10	0.0581	23.9	0.7541	28.8	0.0948	28.8	0.61
JAM_IIIc_54/r	0.93	0.74	0.03	13.18	0.0547	25.5	0.4732	23.1	0.0648	23.0	0.37
JAM_IIIc_56/r	1.39	0.36	0.02	6.21	0.0597	8.5	0.4912	7.8	0.0594	7.5	0.20
JAM_IIIc_57/r	0.51	0.24	0.01	3.68	0.0526	33.0	0.4257	29.7	0.0571	29.7	0.48
JAM_IIIc_59/r	0.76	0.40	0.02	7.24	0.0571	9.9	0.4713	9.0	0.0611	8.9	0.23

Explanations: [a] final blank corrected intensities in μV; [b] final blank corrected intensities in mV; *c* core; *r* rim; *2RSE* 2-sigma relative standard error (in %); *Rho* the error-correlation between the 206/238 and 207/235 ratios

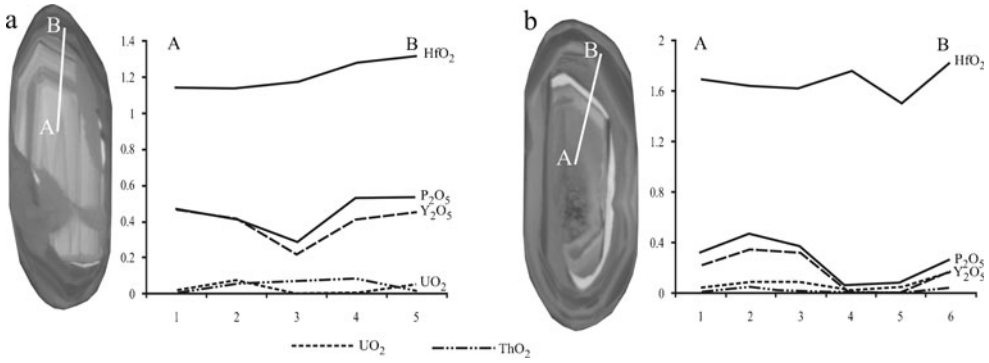

Fig. 10 Electron microprobe traverse across representative zircons from orthogneisses from the Western Tatra Mountains. Concentration are in wt% oxides. Position of the chemical profiles are marked by white line; **a** zircon from sample JAM1; **b** zircon from sample OZ1

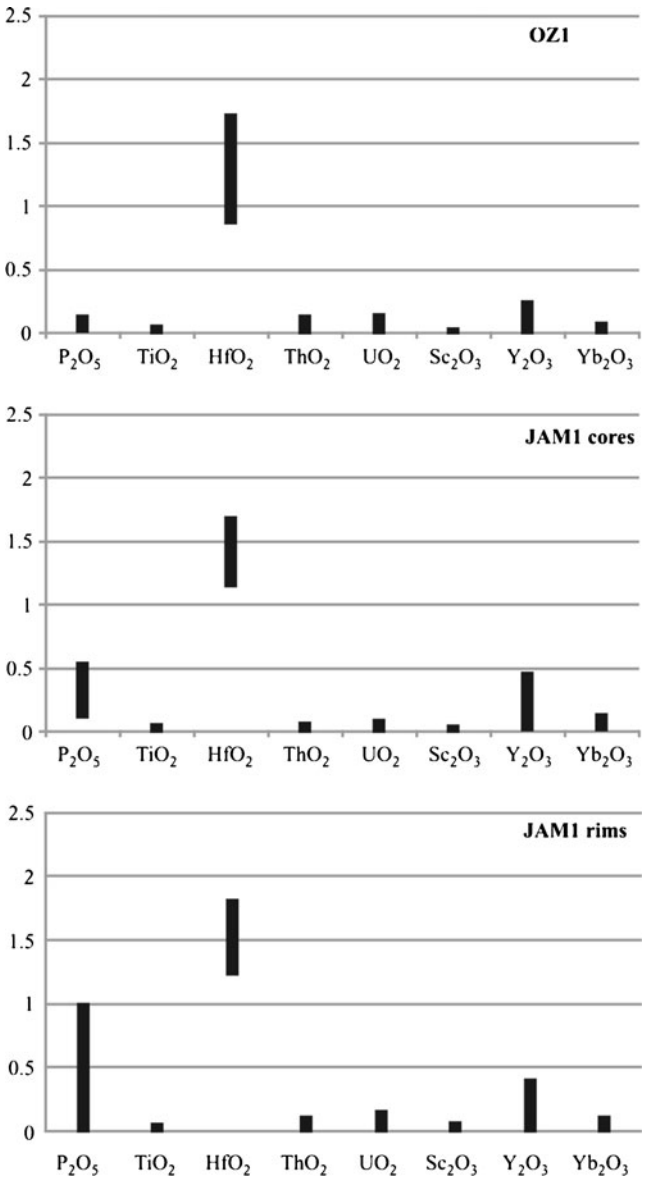

Fig. 11 Compositional comparison between different domains of zircon from the orthogneisses of the Western Tatra Mountains

behaviour of Hf with respect to U, Th and Y can be related to the crystallization of apatite and magnetite before and during zircon growth (Caironi et al. 2000). The late stages of zircon growth seem to have occurred after the complete crystallization of apatite and magnetite. The consequent increased availability of U, Th and Y may explain the observed variation patterns (Fig. 10). The crystallization period of apatite (or other phosphates like monazite) with respect to zircon also influences the coupled substitution $Y^{3+} + P^{5+} \leftrightarrow Zr^{4+} + Si^{4+}$ by removing P from the melt (Caironi et al. 2000).

Our investigations of the orthogneisses from both structural units, with different metamorphic conditions, have shown complexity of zoned zircons that yield both - magmatic protolith and metamorphic ages. Zircon analyses plot in a few age groups (Figs. 6 and 9) corresponding to the associated structures observed in CL images (Figs. 5 and 8).

The oldest, concordant ages of ca. 2.0, 2.2, and 2.6 Ga (Fig. 6a) obtained from short-prismatic, rounded grains with sector zoning (sample OZ1) are interpreted as xenocrysts and are taken as evidence for melting of ancient crustal material involved in magma genesis. The Pan-African and Early Proterozoic/Late Archean ages of these inherited components point to a Gondwanan affinity (West African Craton) for part of the crystalline basement of the Tatra Mountains. The 2.0–2.2 Ga old zircons represent abundant inherited components in the Variscan crust (e.g. Gebauer et al. 1989; Zeck and Williams 2001; Oberc-Dziedzic et al. 2009). A series of magmatic events at the end of the Archean between 2.5 and 2.6 Ga has also been documented for various rocks in the Variscan fold belt (Gebauer et al. 1989; Friedl et al. 2004; Kryza and Zalasiewicz 2008 and refs. therein).

The magmatic cores from sample JAM1 and most zircon crystals from sample OZ1 do not contain any detectable inheritance and yield statistically identical protholith ages at ca. 534 Ma, interpreted as the best estimate for the main magmatic zircon crystallization.

The protolith ages of ca. 534 Ma for the orthogneisses provide strong constraints on the timing of the magmatism recorded in the Tatra massif, placing it almost 130 Ma earlier than previous estimates (Poller et al. 2000). The fact that previous studies have failed to resolve these two growth phases suggests, that their emplacement ages (405 Ma) may be a combination of ca. 534 Ma inherited material and new growth at ca. 387 Ma. Using LA-MC-ICP-MS analysis, sacrificing analytical precision (compared to TIMS) for in situ capability has allowed a better geochronological resolution.

Cambrian ages have previously been reported from other crystalline complexes of the CWC: e.g. 531±29 Ma and 514±24 Ma from ortogneisses from the Low Tatra Mountains (Putiš et al. 2008, 2009). Numerous Paleozoic granite plutons related to the same period of magmatic activity are widespread in vast parts of the Variscan belt of Europe. There are for instance: 513±7, 516±10 and 511±10 Ma for the Teplá crystalline complex in the Bohemian Massif (Dörr et al. 1998), 530–540 Ma for the orthogneisses of the Orlica-Śnieżnik gneisses (Turniak et al. 2000), 542±9 Ma for the Lusatian granodiorites (Tichomirova 2002), 524±10 Ma for Erzgebirge orthogneisses in the Bohemian Massif (Košler et al. 2004) and 530–540 Ma from granodiorites from the NE of the Bohemian Massif (Żelaźniewicz et al. 2004). Their emplacement has been linked to the fragmentation of the northern margin of Gondwana (e.g. Franke 1989; Franke et al. 1996; Matte 1986, 1991; Pin 1990; Oliver et al. 1993; Żelaźniewicz and Franke 1994; Winchester et al. 1995; Kröner and Hegner 1998; Von Raumer 1998; Pin et al. 2007; Kryza and Zalasiewicz 2008).

The rims surrounding the oscillatory zoned cores in JAM1 are interpreted as a phase of new zircon growth at 387±14 Ma, recrystallized under upper amphibolite facies conditions. The external domains could have started to crystallize during incipient dehydration melting. The low Th/U ratios (< 0.1) confirm this growth stage (Schaltegger et al. 1999; Hoskin and Black 2000; Rubatto 2002). The low Th/U could reflect the simultaneous growth of metamorphic minerals rich in Th, or low solubility of Th in the metamorphic fluid (Schaltegger et al. 1999). The fact that these overgrowths preserve not only different zoning and chemistry, but also different ages, proves that they formed in separate stages of the metamorphic evolution of the rock. Similar, Eo-Variscan age is well preserved in outer zircon domains of layered amphibolites and orthogneisses from the Low Tatra Mountains. It is interpreted as indicating the beginning of superimposed metamorphic event due to extensional collapse of the thickened Variscan crust, producing large granitoid pluton (Putiš et al. 2008).

Conclusions

The new geochemical and LA-MC-ICP-MS U-Pb zircon data from orthogneisses from the Western Tatra Mountains provide new constraints to the complex and prolonged history of the Tatra crystalline basement:

1. The ca. 534 Ma concordia age of the oscillatory zoned zircons of both samples is interpreted as the best estimate for the age of the magmatic crystallization of the zircons. The CL images of the zircons yielding this age show typical magmatic textures characterized by a well-defined concentric and oscillatory zoning.
2. This age is interpreted as the intrusion age of the magmatic protolith of the orthogneisses, suggesting that parts of the basement underwent Cadomian tectono-magmatic imprints.
3. These granitoids are interpreted to have been emplaced in an active continental margin of Gondwana. This is the oldest magmatic event identified so far in the crystalline basement of the Tatra Mountains, attaching the evolution of this part of Variscan Europe to the "Galatian terrane" of Von Raumer and Stampfli (2008).
4. The granodiorites from the Upper Unit experienced a subsequent high-grade metamorphic event at ca. 387 Ma, constrained by partial recrystallisation of primary magmatic zircon and growth of new zircon rims. These could be connected with the formation of crustal-scale nappe structures and Eo-Variscan magmatism.
5. Recycling of the Precambrian continental crust, between ca. 2.0–2.6 Ga (Paleoproterozoic-Archean) is indicated by the inherited zircon components from sample OZ1 from the Lower Unit. Similar zircon ages have been detected in samples from the Variscan granitoids of the Tatra Mountains (Burda, unpublished data).
6. The U/Pb zircon geochronology of the pre-Variscan basement rocks of the Western Tatra Mountains confirms their likely West African provenance, as documented by the ages of 1.8–2.2 Ga, and 2.8–3.4 Ga and the absence of Grenvillian zircons.

Acknowledgements The authors would like to thank Jan Košler and Ryszard Kryza who provided detailed and useful reviews of the manuscript. Johann Raith is acknowledged for efficient editorial advice.

This work was financially supported by the Polish Ministry of Sciences and Higher Education (MNiSW grant No. 2 P04D 003 29) and by the Austrian Science Fund FWF (START project 267-N11 and project P18202-N10).

Appendix A

Table 4 Electron microprobe analysis of zircons from sample OZ1. b.d.l. below detection limit

	P_2O_5	SiO_2	TiO_2	ZrO_2	HfO_2	ThO_2	UO_2	Sc_2O_3	Y_2O_3	Yb_2O_3	Total	Zr/Hf
OZ_IV_02/1	0.14	31.77	b.d.l.	66.82	1.00	0.09	0.09	b.d.l.	0.18	0.05	100.15	59
OZ_IV_02/2	0.07	31.75	b.d.l.	66.13	1.42	0.06	0.04	0.02	b.d.l.	0.06	99.63	41
OZ_IV_02/3	0.12	31.76	0.03	66.62	1.42	b.d.l.	b.d.l.	b.d.l.	b.d.l.	0.02	99.98	41
OZ_IV_02/4	0.07	31.74	b.d.l.	66.58	1.41	b.d.l.	0.02	0.04	0.06	b.d.l.	99.92	41
OZ_IV_02/5	0.08	31.59	b.d.l.	66.45	1.36	0.02	b.d.l.	0.01	0.03	b.d.l.	99.54	43
OZ_IV_02/6	0.07	31.45	0.02	66.79	1.28	b.d.l.	0.01	b.d.l.	0.10	0.05	99.77	46
OZ_II b_22/1	0.05	32.29	0.03	66.67	1.30	0.03	0.04	0.02	0.03	0.02	100.47	45
OZ_II b_22/2	0.10	32.19	0.02	65.97	1.34	0.02	b.d.l.	0.01	0.06	0.08	99.80	43
OZ_II b_22/3	0.06	32.41	b.d.l.	65.95	1.46	b.d.l.	b.d.l.	0.01	0.05	0.01	99.97	40
OZ_II b_22/4	0.05	32.10	0.01	66.01	1.39	0.10	b.d.l.	0.02	0.10	0.02	99.81	41
OZ_II b_22/5	0.05	31.83	0.03	64.37	1.72	b.d.l.	0.01	0.03	b.d.l.	b.d.l.	98.06	33
OZ_II b_24/1	0.06	32.35	0.01	66.34	1.35	0.03	0.05	b.d.l.	b.d.l.	b.d.l.	100.23	43
OZ_II b_24/2	0.11	32.25	0.03	66.24	1.27	0.08	0.02	0.02	0.12	b.d.l.	100.14	46
OZ_II b_24/3	0.07	32.14	b.d.l.	66.27	1.41	b.d.l.	b.d.l.	b.d.l.	b.d.l.	0.01	99.89	41
OZ_II b_24/4	0.08	32.25	0.02	66.37	1.21	0.02	0.05	b.d.l.	0.02	0.02	100.04	48
OZ_II b_24/5	0.06	32.28	b.d.l.	66.78	1.24	0.06	0.07	b.d.l.	b.d.l.	b.d.l.	100.49	47
OZ_II b_24/6	0.07	32.13	b.d.l.	66.58	1.39	0.03	b.d.l.	b.d.l.	b.d.l.	0.02	100.20	42
OZ_II b_24/7	0.08	32.05	0.04	66.46	1.29	0.05	0.01	b.d.l.	b.d.l.	b.d.l.	99.99	45
OZ_II b_24/8	0.06	31.86	b.d.l.	66.07	1.33	0.01	0.01	0.01	0.02	0.04	99.41	44
OZ_II b_24/9	0.07	31.89	b.d.l.	66.40	1.29	0.09	0.02	0.02	0.02	0.03	99.81	45
OZ_II b_24/10	0.05	31.48	0.02	65.74	1.28	0.01	b.d.l.	0.01	0.04	b.d.l.	98.62	45
OZ_II b_17/1	0.10	32.15	0.01	66.41	1.22	b.d.l.	0.03	0.01	0.07	0.07	100.10	47
OZ_II b_17/2	0.08	32.14	b.d.l.	66.33	1.22	0.03	0.04	b.d.l.	0.07	0.02	99.94	47
OZ_II b_17/3	0.09	32.13	0.07	66.41	1.20	b.d.l.	0.09	b.d.l.	0.12	0.03	100.14	48
OZ_II b_17/4	0.13	32.20	0.02	65.46	1.23	0.04	0.02	b.d.l.	0.03	b.d.l.	99.14	46
OZ_II b_17/5	0.06	32.26	0.02	66.12	1.35	b.d.l.	0.05	b.d.l.	b.d.l.	0.02	99.89	43
OZ_II b_17/6	0.00	27.29	0.01	42.12	1.65	0.05	0.09	0.01	b.d.l.	0.06	71.27	22
OZ_II b_18/1	0.11	32.19	0.03	66.34	0.86	0.08	0.04	b.d.l.	0.08	0.06	99.79	67
OZ_II b_18/2	0.04	32.26	b.d.l.	65.64	1.29	0.03	b.d.l.	0.01	b.d.l.	b.d.l.	99.28	44
OZ_II b_18/3	0.10	32.41	b.d.l.	65.07	1.22	b.d.l.	0.01	b.d.l.	0.25	0.09	99.15	46
OZ_II b_18/4	0.05	29.99	0.02	28.14	1.24	b.d.l.	b.d.l.	0.01	b.d.l.	0.01	59.47	20
OZ_II b_19/1	0.08	32.29	0.02	66.12	1.29	0.03	0.05	b.d.l.	0.04	0.01	99.94	45
OZ_II b_19/2	0.05	32.15	0.04	66.40	1.35	0.09	0.07	b.d.l.	0.03	0.02	100.20	43
OZ_II b_19/3	0.07	32.10	0.01	66.61	1.36	0.14	0.10	b.d.l.	0.03	b.d.l.	100.42	43
OZ_II b_19/4	0.05	31.74	b.d.l.	66.58	1.49	0.03	0.15	b.d.l.	0.04	0.01	100.10	39
OZ_II b_19/5	0.04	31.46	0.03	66.59	1.28	b.d.l.	0.02	b.d.l.	0.01	0.02	99.45	45

Table 5 Electron microprobe analyses (mass%) of zircons from sample JAM1. *c* core; *r* rim; b.d.l. below detection limit

		P_2O_5	SiO_2	TiO_2	ZrO_2	HfO_2	ThO_2	UO_2	Sc_2O_3	Y_2O_3	Yb_2O_3	Total	Zr/Hf
JAM_Ic_4/146	c	0.47	31.80	0.04	65.19	1.14	b.d.l.	0.03	0.04	0.46	0.08	99.29	50
JAM_Ic_4/147	c	0.42	31.87	0.01	66.50	1.14	0.05	0.08	0.05	0.42	0.08	100.62	51
JAM_Ic_4/148	c	0.29	32.19	0.03	65.38	1.18	0.07	b.d.l.	0.03	0.21	0.05	99.42	49
JAM_Ic_4/149	r	0.53	31.59	0.04	64.88	1.28	0.09	b.d.l.	0.04	0.42	0.09	98.96	44
JAM_Ic_4/150	r	0.42	31.59	0.01	65.68	1.22	0.01	0.05	0.02	0.36	0.09	99.44	47
JAM_Ic_4/152	r	0.08	32.08	b.d.l.	66.74	1.53	0.12	0.05	b.d.l.	b.d.l.	b.d.l.	100.60	38
JAM_Ic_28/153	c	0.33	32.10	0.02	64.89	1.69	b.d.l.	0.04	0.03	0.23	0.10	99.43	34
JAM_Ic_28/154	c	0.47	31.99	0.01	64.96	1.64	0.05	0.09	0.02	0.35	0.13	99.70	35
JAM_Ic_28/155	c	0.38	31.90	0.03	65.22	1.63	b.d.l.	0.09	0.05	0.32	0.13	99.75	35
JAM_Ic_28/156	r	0.00	32.23	0.05	65.56	1.76	b.d.l.	0.02	b.d.l.	b.d.l.	0.04	99.68	33
JAM_Ic_28/157	r	0.10	32.14	b.d.l.	65.65	1.50	b.d.l.	0.04	0.03	b.d.l.	b.d.l.	99.45	38
JAM_Ic_28/158	r	0.27	31.76	0.04	64.10	1.82	0.04	0.17	0.03	0.17	0.06	98.46	31
JAM_Ic_16/159	c	0.11	32.39	0.02	66.14	1.51	b.d.l.	0.03	b.d.l.	b.d.l.	0.01	100.22	38
JAM_Ic_16/160	c	0.31	32.05	0.01	65.84	1.20	0.02	0.04	0.02	0.21	0.07	99.78	48
JAM_Ic_16/161	c	0.34	32.05	0.07	65.74	1.25	0.01	b.d.l.	0.04	0.20	0.06	99.74	46
JAM_Ic_16/162	c	0.40	31.95	0.01	64.98	1.40	b.d.l.	0.02	0.02	0.25	0.07	99.08	40
JAM_Ic_16/163	r	0.33	32.17	0.05	65.47	1.36	0.01	0.03	b.d.l.	0.19	0.10	99.72	42
JAM_Ic_16/164	r	0.29	32.07	b.d.l.	66.13	1.28	0.02	0.01	0.01	0.16	0.02	99.98	45
JAM_Ic_16/165	r	0.33	31.98	0.03	66.49	1.36	b.d.l.	0.03	0.02	0.26	0.07	100.58	43
JAM_Ic_16/166	r	0.37	32.15	0.03	65.76	1.72	0.05	0.07	0.05	0.28	0.07	100.54	33
JAM_Ic_16/167	r	0.49	31.99	0.04	65.52	1.74	0.02	0.10	0.07	0.36	0.12	100.45	33
JAM_Ic_34/168	c	0.33	31.93	0.02	66.04	1.25	b.d.l.	0.05	0.02	0.20	0.03	99.87	46
JAM_Ic_34/169	c	0.32	32.06	0.04	65.46	1.25	0.07	0.01	0.01	0.19	0.03	99.43	46
JAM_Ic_34/170	c	0.29	31.95	b.d.l.	66.27	1.25	b.d.l.	0.02	0.03	0.27	0.08	100.19	46
JAM_Ic_34/171	c	0.48	31.82	b.d.l.	65.88	1.36	b.d.l.	b.d.l.	0.03	0.36	0.14	100.06	42
JAM_Ic_34/172	c	0.55	31.90	0.04	64.91	1.49	b.d.l.	0.05	0.04	0.41	0.09	99.46	38
JAM_Ic_34/173	c	0.31	32.09	0.02	65.17	1.46	b.d.l.	0.03	0.03	0.19	0.05	99.36	39
JAM_Ic_34/174	r	0.11	32.58	0.05	65.63	1.53	b.d.l.	0.07	0.01	0.02	b.d.l.	100.02	37
JAM_Ic_34/175	r	0.14	32.89	0.02	65.75	1.70	0.01	0.07	b.d.l.	0.03	0.03	100.64	34
JAM_Ic_34/176	r	0.08	34.09	0.04	63.39	1.59	b.d.l.	0.01	b.d.l.	b.d.l.	b.d.l.	99.20	35
JAM_IIIc_31/23	c	0.31	32.00	b.d.l.	66.76	1.26	b.d.l.	0.01	0.02	0.17	0.07	100.60	46
JAM_IIIc_31/24	r	0.15	32.43	0.06	66.17	1.66	b.d.l.	0.06	b.d.l.	0.05	0.03	100.62	35
JAM_IIIc_40/25	c	0.16	31.94	0.03	67.29	1.20	b.d.l.	0.01	b.d.l.	0.13	0.07	100.83	49
JAM_IIIc_40/26	c	0.43	31.74	0.04	66.21	1.16	b.d.l.	b.d.l.	0.05	0.28	0.11	100.04	50
JAM_IIIc_40/27	r	0.13	31.76	0.03	67.24	1.51	b.d.l.	0.09	b.d.l.	b.d.l.	b.d.l.	100.81	39
JAM_IIIc_16/28	c	0.26	31.85	0.07	66.70	1.39	b.d.l.	0.05	0.05	0.16	0.06	100.64	42
JAM_IIIc_16/29	r	0.10	31.89	0.04	66.35	1.55	0.02	0.01	0.01	b.d.l.	b.d.l.	99.96	37
JAM_IIIc_16/30	r	0.16	31.89	b.d.l.	66.94	1.47	b.d.l.	0.08	0.02	0.04	b.d.l.	100.61	40
JAM_IIIc_45/31	r	0.15	31.47	b.d.l.	67.05	1.46	0.01	0.09	0.02	0.02	b.d.l.	100.27	40
JAM_IIIc_45/32	r	0.13	31.29	b.d.l.	67.08	1.45	b.d.l.	0.13	0.03	0.04	0.03	100.17	40

References

Bac-Moszaszwili M (1996) The uplift of the Tatra massif in Tertiary and Quaternary. In: The Tatra National Park – Nature and man. Zakopane, Oct. 6th – 9th 1995, Conference proceedings: 68–71

Burchard J (1968) Rubidium-strontium isochron ages of the crystalline core of the Tatra Mountains, Poland. Am J Sci 266(10):895–907

Burda J, Gawęda A (1997) Mass-balance calculations in migmatites from the Upper Kościeliska Valley (The Western Tatra Mts., S-Poland). Miner Pol 28(1):53–68

Burda J, Gawęda A (1999) Petrogenesis of migmatites from the Upper Kościeliska Valley (Western Tatra Mountains). Archiwum Miner 52(2):163–194

Burda J, Gawęda A (2009) Shear-influenced partial melting in the Western Tatra metamorphic complex: geochemistry and geochronology. Lithos 110:373–385

Burda J, Klötzli U (2007) LA-MC-ICP-MS U-Pb zircon geochronology of the Goryczkowa type granite – Tatra Mts., Poland. Pol Tow Mineral Prace Spec 31:89–92

Caironi V, Colombo A, Tunesi A, Gritti C (2000) Chemical variations of zircon compared with morphological evolution during magmatic crystallization: an example from the Valle del Cervo Pluton (Western Alps). Eur J Mineral 12:779–794

Chappell BW, White AJR (1974) Two contrasting granite types. Pac Geol 8:173–174

Dörr W, Fiala J, Vejnar Z, Zulauf G (1998) U–Pb zircon ages and structural development of metagranitoids of the Teplá crystalline complex: evidence for pervasive Cambrian plutonism within the Bohemian Massif (Czech Republic). Int J Earth Sci 87:135–149

Franke W (1989) Tectonostratigraphic units in the Variscan belt of central Europe. Geol Soc Am Spec Pap 230:67–90

Franke W, Fiala J, Haack U, Vejnar Z, Dörr W (1996) The "500 Ma event" in the central Variscides: extension or convergence? Terra Nostra 96:52–54

Friedl G, Ginger F, Paquette JL, Von Quadt A, Mcnaughton NJ, Flechter IR (2004) Pre-Variscan geological events in the Austrian part of the Bohemian Massif deduced from U-Pb zircon ages. Int J Earth Sci 93:802–823

Gawęda A, Kozłowski K, Piotrowska K (1998) Tectonic development of the crystalline basement of the Polish part of the Western Tatra Mts. Acta Universitatis Carolinae – Geologica 42/2:252–253

Gawęda A, Winchester JA, Kozłowski K, Narębski W, Holland G (2000) Geochemistry and paleotectonic setting of the amphibolites from the Western Tatra Mountains. Geol J 35:69–85

Gawęda A, Doniecki T, Burda J, Kohut M (2005) The petrogenesis of quartz-diorites from the Tatra Mountains (Central Western Carpathians): an example of magma hybridisation. N Jb Miner Abh 181(1):95–109

Gebauer D, Williams IS, Compston W, Grunenfelder M (1989) The development of the Central European continental crust since the Early Archean based on convenctional and ion microprobe dating of up 3,84 b.y. old detrital zircons. Tectonophysics 157:81–96

Griffin WL, Wang X, Jackson SE, Pearson NJ, O'Reilly SY, Xu X, Zhou X (2002) Zircon chemistry and magma genesis, SE China: in-situ analysis of Hf isotopes, Pingtan and Tonglu igneous complexes. Lithos 61:237–269

Hoskin PWO (2005) Trace-element composition of hydrothermal zircon and the alteration of Hadean zircon from the Jack Hills, Australia. Geochim Cosmochim Acta 69:637–648

Hoskin PWO, Black LP (2000) Metamorphic zircon formation by solid state recrystallization of protolith igneous zircon. J Metamorph Geol 18:423–439

Janák M, O'Brien PJ, Hurai V, Reutel C (1996) Metamorphic evolution and fluid composition of garnet-clinopyroxene amphibolites from the Tatra Mountains, Western Carpathians. Lithos 39:57–79

Kohút M, Janak M (1994) Granitoids of the Tatra Mts., Western Carpathians: field relations and petrogenetic implications. Geol Carpathica 45(5):301–311

Kohút M, Poller U, Gurk C, Todt W (2008) Geochemistry and U-Pb detrital zircon ages of metasedimentary rocks of the Lower Unit, Western Tatra Mountains (Slovakia). Acta Geologica Polonica 58:371–384

Košler J, Bowes DR, Konopàsek J, Mìková J (2004) Laser ablation ICPMS dating of zircons in Erzgebirge orthogneisses: evidence for Early Cambrian and Early Ordovician granitic plutonism in the western Bohemian Massif. Eur J Mineral 16:15–22

Krist E, Korikovsky SP, Putiš M, Janak M, Faryad SW (1992) Geology and petrology of metamorphic rocks of the Western Carpathian crystalline complexes. Comenius University Press, Bratislava, pp 1–324

Kröner A, Hegner E (1998) Geochemistry, single zircon ages and Sm–Nd systematics of granitoid rocks from the Gory Sowie (Owl Mts), Polish West Sudetes; evidence for early Paleozoic arc-related plutonism. J Geol Soc Lond 155:711–724

Kryza R, Zalasiewicz J (2008) Records of Precambrian - Early Palaeozoic volcanic and sedimentary processes in the Central European Variscides: a review of SHRIMP zircon data from the Kaczawa succession (Sudetes, SW Poland). Tectonophysics 461:60–71

Ludwig KR (2003) Isoplot/Ex version 3.00. A geochronological toolkit for Microsoft Excel. Berkeley Geochronology Center. Special Publication No. 4

Marc D (1992) Granites and rhyolites from the northwestern USA: temporal variation in magmatic processes and relations to tectonic setting. Trans R Soc Edinb-Earth Sci 83:51–64

Matte P (1986) Tectonics and plate tectonics model for the Variscan belt of Europe. Tectonophysics 126:329–374

Matte P (1991) Accretionary history and crustal evolution of the Variscan belt in western Europe. Tectonophysics 196:309–337

O'Connor JT (1965) A classification for quartz-rich igneous rocks based on feldspar ratios. US Geol Surv Prof Pap B 525:79–84

Oberc-Dziedzic T, Kryza R, Pin C (2009) The crust beneath the Polish Sudetes: evidence from a gneiss xenolith in Tertiary basanite from Paszowice. Geodinamica Acta 22(3):9–31

Oliver GJH, Corfu F, Krogh TE (1993) U–Pb ages from SW Poland, evidence for a Caledonia structure zone between Baltica and Gondwana. J Geol Soc Lond 150:355–369

Pearce JA, Harris NJ, Tindle AG (1984) Trace element discrimination for the tectonic interpretation of granitic rocks. J Petrol 25:956–983

Pérez-Soba C, Villaseca C, Gonzáles del Tánago J, Nasdala L (2007) The composition of zircon in the peraluminous Hercynian granites of the Spanish Central System batholith. Can Mineral 45:509–527

Pin C (1990) Variscan oceans: ages, origins and geodynamic implications inferred from geochemical and radiometric data. Tectonophysics 177:215–227

Pin C, Kryza R, Oberc-Dziedzic T, Mazur S, Turniak K, Waldhausrova J (2007) The diversity and geodynamic significance of Late Cambrian (ca. 500 Ma) felsic anorogenic magmatism in the northern part of the Bohemian Massif: a review based on Sm–Nd isotope and geochemical data. In: Linnemann U, Nance D, Kraft P, Zulauf G (eds). The evolution of the Rheic ocean: from avalonian-cadomian active margin to Alleghenian-Variscan collision. Geol Soc Am Spec Pap 423:209–229

Poller U, Janak M, Kohút M, Todt W (2000) Early Variscan magmatism in the Western Carpathians: U-Pb zircon data from granitoids and orthogneisses of the Tatra Mountains, Slovakia. Int J Earth Sci 89:336–349

Poller U, Todt W, Kohút M, Janak M (2001a) Nd, Sr, Pb isotope study of the Western Carpathians: implications for the Paleozoic evolution. Schweiz Miner Petrol Mitt 81:159–174

Poller U, Huth J, Hoppe P, Williams IS (2001b) REE, U, Th and Hf distribution in zircon from Western Carpathian Variscan granitoids: a combined cathodoluminescence and ion microprobe study. Am J Sci 301:858–876

Putiš M, Sergeev S, Ondrejka M, Larionov A, Siman P, Spišiak J, Uher P, Paderin I (2008) Cambrian-Ordovician metaigneous rocks associated with Cadomian fragments in the West-Carpathian basement dated by SHRIMP on zircons: a record from the Gondwana active margin setting. Geol Carpathica 59 (1):3–18

Putiš M, Ivan P, Kohút M, Spišiak J, Siman P, Radvanec M, Uher P, Sergeev S, Larionov A, Méres Š, Rastislav Demko R, Ondrejka M (2009) Meta-igneous rocks of the West-Carpathian basement,

Slovakia: indicators of Early Paleozoic extension and shortening events. Bull Soc Geol Fr 180(6):461–471

Rubatto D (2002) Zircon trace element geochemistry: partitioning with garnet and the link between U–Pb ages and metamorphism. Chem Geol 184:123–138

Schaltegger U, Fanning CM, Günther D, Maurin JC, Schulmann K, Gebauer D (1999) Growth, annealing and recrystallization of zircon and preservation of monazite in high-grade metamorphism: conventional and in situ U–Pb isotope, cathodoluminescence and microchemical evidence. Contrib Mineral Petrol 134:186–201

Slama J, Kosler J, Schaltegger U, Tubrett M, Gutjahr M (2006) New natural zircon standard for laser ablation ICP-MS U-Pb geochronology. Abstract WP05. Winter Conference on Plasma Spectrochemistry, Tucson: 187–188

Stacey JS, Kramers JD (1975) Approximation of terrestrial lead isotope evolution by a two stage model. Earth Planet Sci Lett 26:207–221

Sun SS, McDonough WF (1989) Chemical and isotopical systematics of oceanic basalts: implications for mantle composition and processes. Magmatism in the Oceanic Basins. Geol Soc Spec Publ 42:313–345

Sylvester PJ, Ghaderi M (1997) Trace element analysis of scheelite by excimer laser ablation–inductively coupled plasma–mass spectrometry (ELA–ICP–MS) using a synthetic silicate glass standard. Chem Geol 141:49–65

Tichomirova M (2002) Zircon inheritance in diatexite granodiorites and its consequence on geochronology – a case study in Lusatia and Erzgebirge (Saxo-Thuringia, eastern Germany). Chem Geol 191:209–224

Turniak K, Mazur S, Wysoczański R (2000) SHRIMP zircon geochronology and geochemistry of the Orlica-Śnieżnik gneisses (Variscan belt of Central Europe) and their tectonic implications. Geodinamica Acta 13:293–312

Vavra G, Schmid R, Gebauer D (1999) Internal morphology, habit and U-Th-Pb microanalysis of amphibolite-to-granulite facies zircons: geochronology of the Ivrea Zone (Southern Alps). Contrib Mineral Petrol 134:380–404

Von Raumer JF (1998) The Palaeozoic evolution in the Alps: from Gondwana to Pangea. Int J Earth Sci 87:407–435

Von Raumer JF, Stampfli GM (2008) The birth of the Rheic Ocean - Early Paleozoic subsidence patterns and subsequent tectonic plate scenarios. Tectonophysics 461:9–20

Whitehouse MJ, Platt JP (2003) Dating highgrade metamorphism – constraints from rare-earth elements in zircon and garnet. Contrib Mineral Petrol 145:61–74

Whitney DL, Evans BW (2010) Abbreviations for names of rock-forming minerals. Am Mineral 95:185–187

Wiedenbeck M, Alle P, Corfu F, Griffin WL, Meier M, Oberli F, Von Quadt A, Roddick JC, Spiegel W (1995) Three natural zircon standards for U-Th-Pb, Lu-Hf, trace element and REE analyses. Geost Newslet 19:1–23

Williams IS, Buick IS, Cartwright I (1996) An extended episode of early Mesoproterozoic metamorphic fluid flow in the Reynolds Range, central Australia. J Metamorph Geol 14:29–47

Winchester JA, Floyd PA, Chocyk M, Horbowy K, Kozdroj W (1995) Geochemistry and tectonic environment of Ordovician meta-igneous rocks in the Rudawy Janowickie Complex, SW Poland. J Geol Soc 152:105–115

Zeck HP, Williams IS (2001) Inherited and magmatic zircon from Neogene Hoyazo cordierite dacite, SE Spain—Anatectic source rock provenance and magmatic evolution. J Petrol 43:1089–1104

Żelaźniewicz A, Franke (1994) Discussion on U–Pb ages from SW Poland: evidence for a Caledonian suture zone between Baltica and Gondwana. J Geol Soc Lond 151:1050–1052

Żelaźniewicz A, Dörr W, Bylina P, Franke W, Haack U, Heinisch H, Schastok J, Grandmontagne K, Kulicki C (2004) The eastern continuation of the Cadomian orogen: U-Pb zircon evidence from Saxo-Thuringian granitoids in south-western Poland and the northern Czech Republic. Int J Earth Sci 93:773–781